Bioorganic & Medicinal Chemistry Letters 20 (2010) 2287–2291

Contents lists available at ScienceDirect

Bioorganic & Medicinal Chemistry Letters

journal homepage: www.elsevier.com/locate/bmcl

Gold nanoparticles functionalized by gadolinium–DTPA conjugate of cysteine as a multimodal bioimaging agent

Ji-Ae Park [a], Hee-Kyung Kim [b], Joo-Hyun Kim [b], Sang-Won Jeong [c], Jae-Chang Jung [d], Gang-Ho Lee [e], Jongmin Lee [b,f], Yongmin Chang [b,f,*], Tae-Jeong Kim [g,*]

[a] Laboratory of Nuclear Medicine Research, Molecular Imaging Center, Korea Institute of Radiological and Medical Science, Seoul, Republic of Korea
[b] Department of Medical and Biological Engineering, Kyungpook National University, Daegu, Republic of Korea
[c] BT Division, DGIST, Daegu, Republic of Korea
[d] Department of Biology, Kyungpook National University, Daegu, Republic of Korea
[e] Department of Chemistry, Kyungpook National University, Daegu, Republic of Korea
[f] Department of Diagnostic Radiology and Molecular Medicine, Kyungpook National University, Daegu, Republic of Korea
[g] Department of Applied Chemistry, Kyungpook National University, Daegu, Republic of Korea

ARTICLE INFO

Article history:
Received 8 December 2009
Revised 23 January 2010
Accepted 1 February 2010
Available online 6 February 2010

Keywords:
Gadolinium chelate
Gold nanoparticles
MRI-CT bimodality
T1 agent
DTPA–cysteine

ABSTRACT

The synthesis and characterization of gold nanoparticles coated with Gd-chelate (Au@GdL), where L is a conjugate of DTPA and cysteine, is described. These particles are obtained by the replacement of citrate from the gold nanoparticle surfaces with gadolinium chelate (GdL). The average size of Au@GdL is 14 nm with a loading of GdL reaching up to 2.9×10^3 per particles, and they demonstrate very high R1 relaxivity ($\sim 10^5$ mM^{-1} s^{-1}) as well as X-ray attenuation. The R1 relaxivity per [Gd] is 17.9 mM^{-1} s^{-1}. The present system also exhibits macrophage-specific property, as demonstrated by histological and TEM images as well as CT and MR, rendering itself as a new class of T1 multimodal CT/MR contrast agent.

MRI is a popular technique in that it has a good soft tissue contrast and high spatial resolution (micrometer rather than several millimeters) with non-invasive in vivo visualization. Paramagnetic Gd-chelates are the most widely administered contrast agent (CA) to improve the contrast in the MR image by shortening the T1-relaxation times of the water proton.[1] Recently, in an effort to design more effective Gd-based T1 MRI CAs, a new approach leading to the formation of gadolinium nanoparticles (GdNPs) has been developed, since their relaxivities are much higher than those of clinically approved Gd-chelates.[2] A representative example includes water-soluble apoferritin-encapsulated GdNPs with T1 and T2 relaxivities much higher than those of classic Gd(III)-complexes (10–25 and 70 times, respectively).[3] Another recent effort has been directed toward the development of multifunctional imaging modalities such as PET/CT, SPECT/CT, MRI/PET, and MRI/optical.[4] Along with this effort, various paramagnetic nanomaterials with multifunctional modality have also emerged. For instance, hybrid nanoparticles consisting of $Gd_2O(CO_3)_2 \cdot H_2O$/silica/gold and gold nanoparticles coated with GdL have been reported as bifunctional agents for MRI/photothermal destruction of cancer cells.[5]

In contrast to the availability of such diverse multifunctional imaging modalities as mentioned above, MR/CT bimodality has rarely been explored although the two techniques are separately applied to the same patient to improve the accuracy of diagnosis or assess the efficacy of treatment routines. CT, which is one of the most useful diagnostic tools in terms of frequency of use and cost, has high spatial resolution and good hard tissue contrast. Current CAs for CT are based on iodinated small molecules because, among nonmetal atoms, iodine has a high X-ray absorption coefficient.[6]

Iodinated compounds, however, allow only very short imaging times due to rapid clearance by the kidney, which can also cause them to have renal toxicity. In this regard, it is worth noting that novel nanoparticle-based CT CAs has recently emerged to overcome the shortcomings of iodine-based agents. Gold nanoparticles (AuNPs), for instance, have demonstrated a great potential as an excellent substitute for iodine.[7] The employment of AuNPs in CT offer some unique advantages in that gold has a higher X-ray absorption coefficient than iodine (5.16 and 1.94 cm^2/g, respectively, at 100 keV) and at the same time biocompatible and

* Corresponding authors.
E-mail addresses: ychang@knu.ac.kr (Y. Chang), tjkim@knu.ac.kr (T.-J. Kim).

0960-894X/$ - see front matter © 2010 Elsevier Ltd. All rights reserved.
doi:10.1016/j.bmcl.2010.02.002

nontoxic in vivo. Furthermore, an additional advantage of AuNPs comes from the fact that facile surface modification may lead to the formation of various functionalities applicable to multiple imaging modalities such as MRI/CT.

In this regard, it is worth to note that Roux has recently demonstrated for the first time that AuNPs coated with paramagnetic Gd(DTDTPA), Au@Gd(DTDTPA), is an attractive bimodal MRI/CT CA.[8] The study reveals that Au@Gd(DTDTPA) may be in many respects a substitute for commercially available, low molecular weight Gd(III)-based MRI CAs. For example, R1 relaxivity of Au@Gd(DTDTPA) is nearly the same as that of Omniscan® to give 3.90 mM^{-1} s^{-1}, and its size is small enough (2–2.5 nm) to freely circulate in the blood vessels without being accumulated in the organs such as lungs, spleen, and liver.

Yet, considering the fact that most of MRI CAs currently on the market are extracellular and non-specific with low relaxivities, development of bimodal MRI/CT CAs with high relaxivity as well as organ specificity is highly desirable. Intrigued by the work of Roux and motivated by our continued effort to develop a new class of bifunctional MRI/CT CAs,[9] herein we report the synthesis and in vivo application of AuNPs coated with Gd-complex of DTPA-bis(amide) conjugate of cysteine, Au@GdL.

The final product Au@GdL was prepared according to the method described elsewhere with a slight modification (Scheme 1).[10] The ligand (L), a conjugate of DTPA with cysteine, was prepared straightforwardly from the reaction of DTPA-bis(anhydride) with 2 equiv of cysteine in DMF at 80 °C for 6 h. The subsequent reaction of L with Gd_2O_3 in water under reflux led to the formation of GdL as a white solid. The coating of AuNPs with GdL was accomplished by direct addition of an aqueous solution of GdL to a solution of citrate-coated AuNPs with a size of ~12 nm. Stirring was continued for 24 h before Au@GdL nanoparticles were collected by centrifugation and washed successively with water, acetone, and ether.

The formation of GdL as $[Gd(L)(H_2O)]\cdot xH_2O$ and Au@GdL was confirmed by analytical and spectroscopic techniques. The MALDI-TOF mass spectrum exhibits the molecular peak at 783 Da corresponding to $[M]^+ - H_2O$ (Fig. S1, Supplementary data). Figure 1(A) shows the TEM image of well-dispersed spherical particles of Au@GdL. The particles have a mean size of 14 nm with a narrow size distribution. Figure 1(B) shows the powder X-ray diffraction pattern typical for AuNPs. Namely, the peaks at 38.2°, 44.4°, 64.5°, 77.5°, and 81.7° correspond to the planes of (1 1 1), (2 0 0), (2 2 0), (3 1 1), and (2 2 2), respectively.[11]

The visible absorption spectrum shows a band at ca. 540 nm corresponding to the excitation of surface plasmon vibrations of mono-dispersed gold nanoparticles confirming the formation of AuNPs (Fig. S2).[12]

GdL may bind to AuNPs in various modes as illustrated in Scheme 1 as thiols in GdL may undergo air-oxidation to form disulfide bonds. The same observation has also been reported with analogous Au@Gd(DTDTPA).[8] The binding of GdL to the AuNPs surface can be confirmed by FT-IR (Fig. S3). The S–H stretching band at 2550 cm^{-1} in GdL (curve a) is absent by the formation of Au@GdL (curve b). Other conspicuous change found in the IR spectrum of Au@GdL is that the bands in the range of 1500–2000 cm^{-1} are reduced in intensity. A probable implication is that the carboxylic groups in GdL may also be involved in the binding to the gold surface.[13]

The concentration of gadolinium as well as the number of GdLs per AuNP was determined by inductively coupled plasma mass spectrometry (ICP-MS) for Gd and Au following the procedure reported earlier.[14] Namely, determination of the gold concentration followed by theoretical calculation based on the average size of 14 nm reveals the total number of GdLs per AuNP to be about 2.9×10^3. A further confirmation of such a high loading of GdL comes from the TGA results which show the weight loss of 5.6% in the temperature range 100–800 °C, corresponding to the decomposition of the organic ligand (Fig. S4). This value matches well with the total number of GdLs per nanoparticle calculated based on the ICP data. Such a number of GdLs per AuNP is extremely high

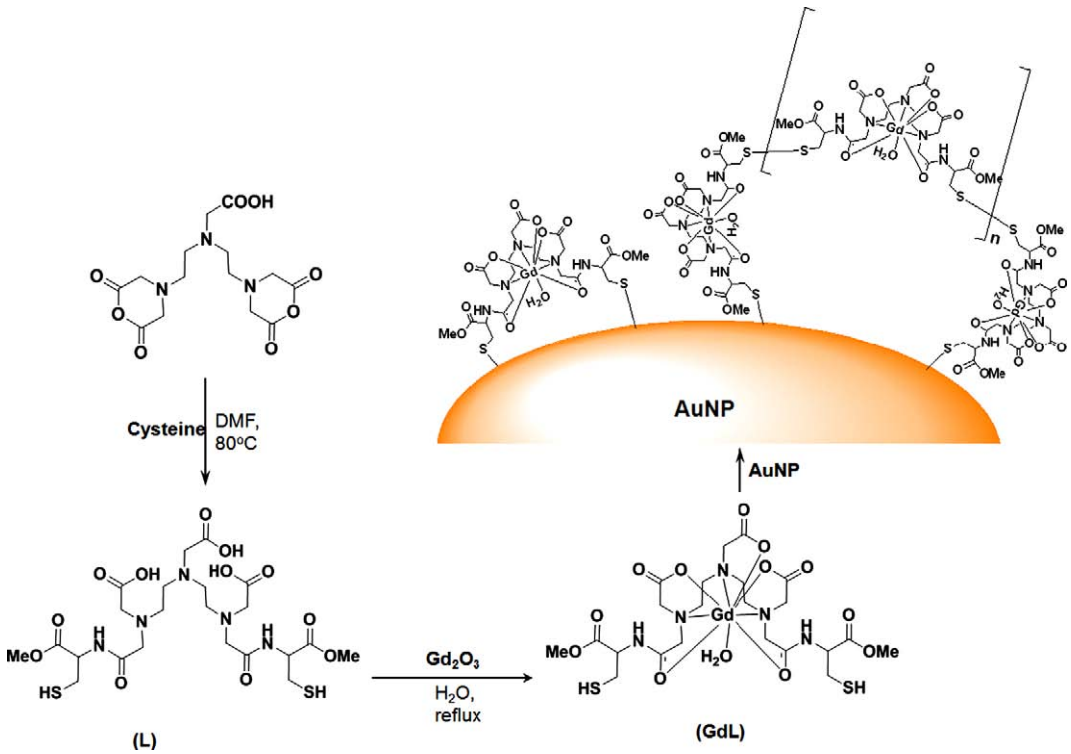

Scheme 1.

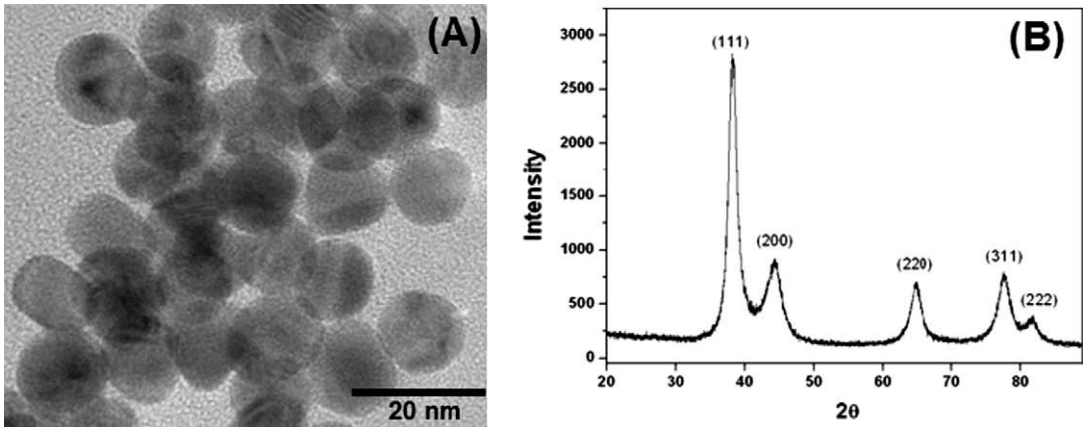

Figure 1. Characterization of Au@GdL: (A) TEM images and (B) powder X-ray diffraction pattern.

and almost 20-times as high as those found with analogous systems.[8] Higher degree of oligomerization of thiols in L may be a partial explanation for such a high loading of gadolinium. The zeta potential of AuGdL is −41.03 mV at pH 6.0 in water (Fig. S5), and negatively large enough to ensure a colloidal stability.

Figure 2 shows plots of in vitro X-ray attenuation of Au@GdL, Au@L, and Ultravist® as a function of concentration. As expected, both Au@GdL and Au@L exhibit higher attenuation than Ultravist®, a clinically used iodine-based CT CA; the differences become greater as the concentration increases. For instance, at the concentration of 200 mM, both nanoplatforms show the attenuation almost three times as high as that of Ultravist®. When the comparison is made between Au@GdL and Au@L, the former shows the higher attenuation, demonstrating a synergistic effect of gadolinium. The coherent in vivo data are provided in Figure S6. Quantitatively, an extra contrast enhancement of about 15% seems to be contributed by 2 wt% of gadolinium immobilized on AuNPs. It is well known that gadolinium, although possessing a lower X-ray absorption coefficient (3.11 cm^2/g at 100 keV) than gold, exhibits much stronger absorption than iodine.[15] These observations clearly indicate that Au@GdL may be employed in vivo as a highly efficient CT agent.

Figures 3 and 4 show in vivo CT images and X-ray attenuation profiles, respectively, of mice obtained with Au@GdL. A dose of 1.75 mmol [Au]/kg body weight was injected to the tail vein of mice and the images monitored up to 360 min after injection. All organs show clear contrast enhancement with Au@GdL, and the most dramatic enhancement is observed in the liver. These observations are the ones that can be typically expected for AuNPs with the size of 10–13 nm.[16] Figure 3 shows the maximum attenuation in the liver to reach up to five-times as high as that of pre-injection and sustain in the same level as long as 6 h after injection. It is likely that the majority of Au@GdL may have accumulated in the Kupffer cells of the liver although some have accumulated in kidney and spleen as a result of glomerular filtration function and macrophage activity, respectively.[17]

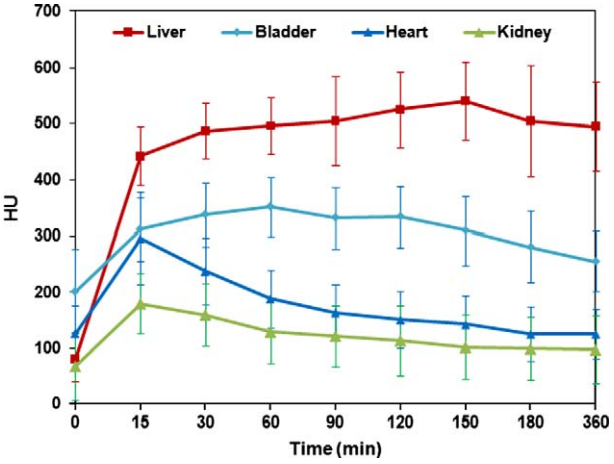

Figure 3. In vivo X-ray attenuation profiles as a function of time from mice.

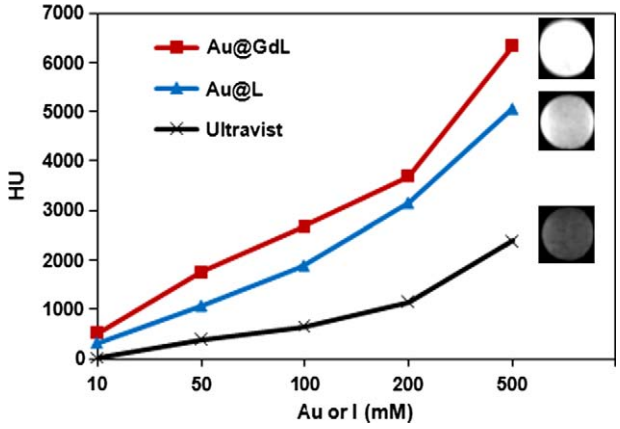

Figure 2. Plots of in vitro X-ray attenuation (in HU) as a function of concentration of gold or iodine and phantom images at 500 mM.

Here it is worth noting that Au@GdL is in a striking contrast with Au@Gd(DTDTPA) in that the latter exhibits dominant kidney enhancement.[8] These differences including the improved bio-distribution pattern with Au@GdL may be explained in terms of the difference in the mean particle size; that is, Au@Gd(DTDTPA) is too small (~2.4 nm) to possess multi-organ specificity, and therefore excreted mostly through kidney. The bio-distribution pattern characteristic of Au@Gd(DTDTPA) is the same as that of conventional iodine-based CT CAs. Undesirable accumulation in the organ may be considered as one of advantages of Au@Gd(DTDTPA), yet it could constitute a handicap in that little diagnostic information may be obtained due to too rapid pharmacokinetics. Au@GdL, on the other hand, is large enough (14 nm) to be taken up by Kupffer cells of the liver, and yet at the same time small enough to be filtered by kidney. This size has further implication on the blood-pool effect of Au@GdL as observed in connection with MRI (vide infra).

The accumulation of Au@GdL in Kupffer cells can be further demonstrated by both histological and TEM images provided in Figure 5(A) and (B), respectively.

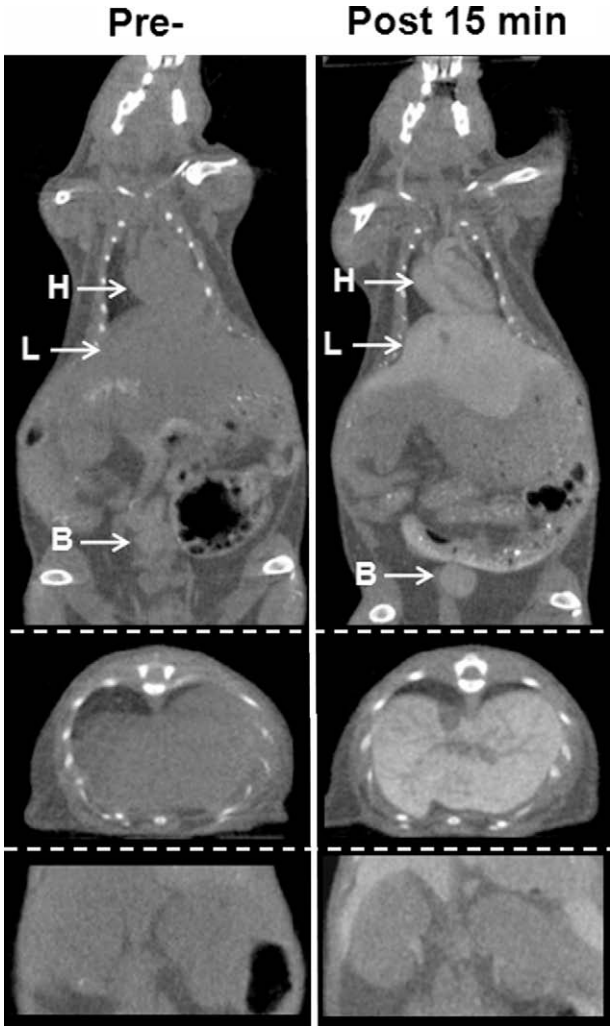

Figure 4. In vivo CT coronal images of mice injected with Au@GdL: H, heart; L, liver; B, bladder (up), axial images of liver (middle), and coronal images of kidney (down).

Table 1 lists R1 relaxivity data for Omniscan®, GdL, and Au@GdL measured at 293 K and 1.5 T. The R1 relaxivity of GdL is twice as high as that of Omniscan®, probably due to higher molecular weight of GdL. The same R1 relaxivity increases dramatically up to 17.9 mM^{-1} s^{-1} by the formation of Au@GdL. This observation is quite remarkable in that such a huge increase is not observed with the related nanosystem, Au@Gd (DTDTPA).[8a,b] When calculated in terms of the AuNP concentration, the molecular R1 relaxivity is 4.6×10^5. This value is exceptionally high in a system where paramagnetic GdL is immobilized on a solid support, and compares well with those of a hybrid nanoparticle system having multiple layers of Gd–DTTA.[18] Such a high relaxivity demonstrated by Au@GdL may partially be rationalized in terms of slower tumbling motion of GdL on AuNPs due to the formation of rigid oligomeric framework resulted from disulfide bonds (cf. Scheme 1).

Table 1
Relaxivity[a] data of Au@GdL

CA (mM)	R1 ($mM^{-1}s^{-1}$)	R2 ($mM^{-1}s^{-1}$)
Omniscan®	3.30 ± 0.02	3.8 ± 0.06
GdL	7.5 ± 0.08	12.3 ± 0.21
Au@GdL: [Gd]	17.9 ± 1.1	28.2 ± 1.0
Au@GdL: [AuNP]	4.6×10^5	7.2×10^5

[a] Relaxivity measured at 293 K and 1.5 T.

Figure 6 shows in vivo MR coronal images of mice obtained with Au@GdL. A dose of 0.03 mmol [Gd]/kg body weight was administrated via the tail vein and the images monitored up to 240 min after injection. Here again, in line with the observations made with CT images, a strong signal enhancement specifically in the liver is seen with Au@GdL. An additional point to highlight in connection with Au@GdL is the prolonged high signal enhancement of abdominal aorta with its long-circulating blood-pool effect. AuNPs with the size of approximately 15 nm are known to exhibit notable ability of recirculation and consequently higher concentration in blood for a longer period than their counterparts with larger sizes (~50–160 nm).[17a]

This is for the first time that T1 MRI CA such as Au@GdL exhibit such high accumulation in the liver in a similar way as ultra-small superparamagnetic iron oxide (USPIO), a well known liver-specific T2 MRI CA.[19]

The cytotoxicity assay was performed with Au@GdL using 14D Chick cornea stroma primary cells and NIH-3T3 mouse embryonic fibroblast cells. Figure S7 shows no obvious decrease of cell viability when the cells are exposed for 24 h in the concentration range of 10–1000 μM of Au@GdL. The relative cell viability increases with an increase in the concentration of Au@GdL. The observation such as this has already been reported in the literature.[20] Such a seemingly odd behavior may be explained in terms of cell prolifer-

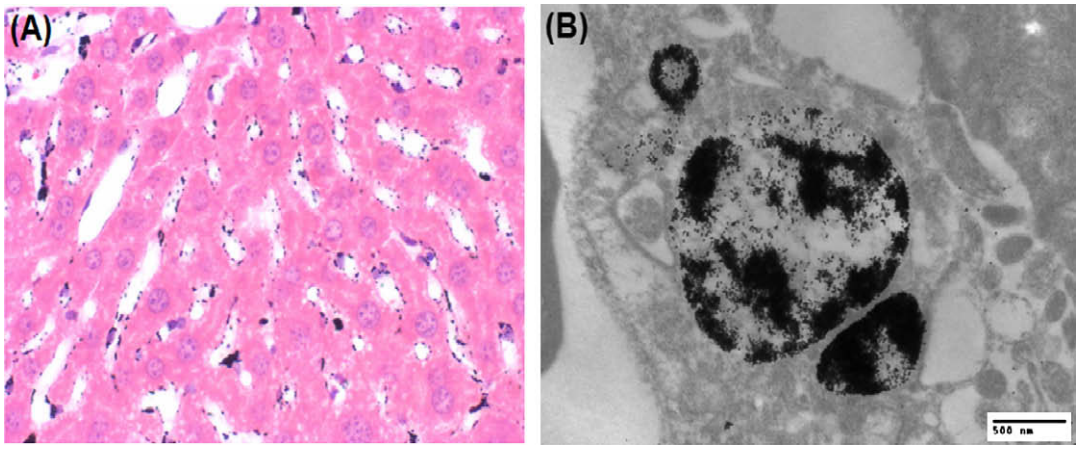

Figure 5. Histological (magnification: 400×) (A) and TEM (magnification: 5000×) (B) images of Kupffer cells of mouse liver after intravenous administration of Au@GdL. The TEM image shows Au@GdL entrapped in lysosomes.

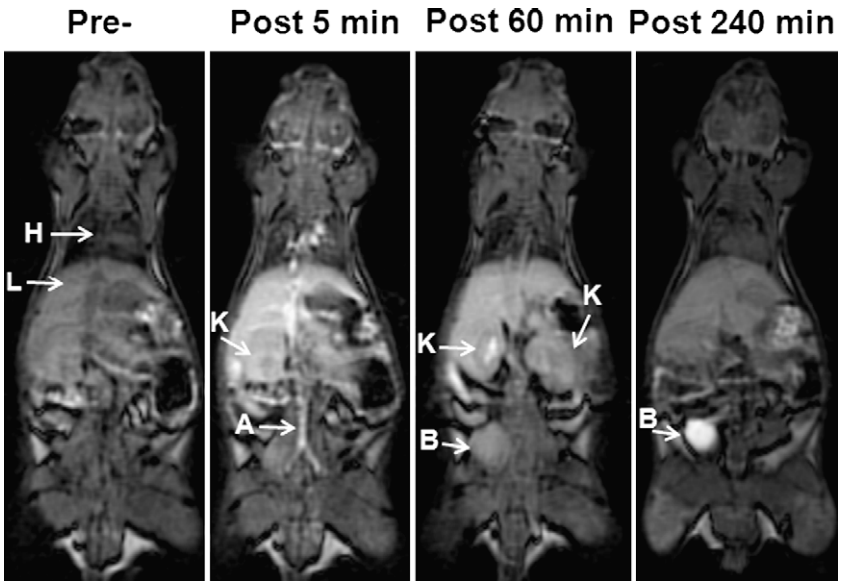

Figure 6. In vivo MR coronal images of mice obtained with Au@GdL: H, heart; L, liver; K, kidney; A, abdominal aorta; B, bladder.

ation stimulated by Au@GdL in the given concentration range.[21] The MTT results demonstrate that Au@GdL has very low cytotoxicity to be used for practical application.

We have described the synthesis of gold nanoparticles coated with Gd-chelate, Au@GdL, where L is a conjugate of DTPA and cysteine, for use as a potential bimodal CT/MR contrast agent. Characterization of these particles by HRTEM, XRD, TGA, and ICP reveals that the size of Au@GdL is 14 nm with the loading of GdL on AuNPs reaching up to 2.9×10^3 GdL per AuNP. Extremely high molecular R1 relaxivity ($\sim 10^5\ mM^{-1}\ s^{-1}$) as well as X-ray attenuation has been accomplished with Au@GdL. The R1 relaxivity per [Gd] is as high as $17.9\ mM^{-1}\ s^{-1}$. A synergistic effect of gadolinium in Au@GdL on X-ray attenuation has been confirmed. Most significantly, the macrophage-specific nature of Au@GdL is demonstrated as documented by in vivo MR, CT, and histological and TEM images.

Acknowledgments

Financial support from The Advanced Medical Technology Cluster for Diagnosis & Prediction, KNU from MKE, ROK (Grant No. RTI04-01-01) is gratefully acknowledged. The MEST/NRF is also acknowledged for the financial support through the Nuclear R&D Program. Nuclear R&D Program (Grant code: 20090081817) of NRF funded by MEST. Spectral measurements were performed by the KBSI.

Supplementary data

Supplementary data associated with this article can be found, in the online version, at doi:10.1016/j.bmcl.2010.02.002.

References and notes

1. Caravan, P.; Ellison, J. J.; McMurry, T. J.; Lauffer, R. B. *Chem. Rev.* **1999**, *99*, 2293.
2. (a) Aime, S.; Botta, M.; Fasano, M.; Geninatti Crich, S.; Terreno, E. *Coord. Chem. Rev.* **1999**, *185*, 321; (b) Reynolds, C. H.; Annan, N.; Beshah, K.; Huber, J. H.; Shaber, S. H.; Lenkinski, R. E.; Wortman, J. A. *J. Am. Chem. Soc.* **2000**, *122*, 8940.
3. Sánchez, P.; Valero, E.; Gálvez, N.; Domínguez-Vera, J. M.; Marinone, M.; Poletti, G.; Corti, M.; Lascialfari, A. *Dalton Trans.* **2009**, 800.
4. Kim, J.; Kim, H. S.; Lee, N.; Kim, T.; Kim, H.; Yu, T.; Song, I. C.; Moon, W. K.; Hyeon, T. *Angew. Chem.* **2008**, *47*, 8438.
5. (a) Hu, K.-W.; Jhang, F.-Y.; Su, C.-H.; Yeh, C.-S. *J. Mat. Chem.* **2009**, *19*, 2147; (b) Lim, Y. T.; Cho, M. Y.; Choi, B. S.; Lee, J. M.; Chung, B. H. *Chem. Commun.* **2008**, 4930.
6. Fenchel, S.; Fleiter, T. R.; Aschoff, A. J.; Gessel, R. V.; Brambs, H.-J.; Merkle, E. M. *Br. J. Radiol.* **2004**, *77*, 821.
7. (a) Kattumuri, V.; Katti, K.; Bhaskaran, S.; Boote, E. J.; Casteel, S. W.; Fent, G. M.; Robertson, D. J.; Chandrasekhar, M.; Kannan, R.; Katti, K. V. *Small* **2007**, *3*, 333; (b) Cai, Q.-U.; Kim, S. H.; Choi, K. S.; Kim, S. Y.; Byun, S. J.; Kim, K. W.; Park, S. H.; Juhng, S. K.; Yoon, K.-H. *Invest Radiol.* **2007**, *42*, 797.
8. (a) Debouttiere, P.-J.; Roux, S.; Vocanson, F.; Billotey, C.; Beuf, O.; Favre-Reguillon, A.; Lin, Y.; Pellet-Rostaing, S.; Lamartine, R.; Perriat, P.; Tillement, O. *Adv. Funct. Mater.* **2006**, *16*, 2330; (b) Alric, C.; Taleb, J.; Duc, G. L.; Mandon, C.; Billotey, C.; Meur-Herland, A. L.; Brochard, T.; Vocanson, F.; Janier, M.; Perriat, P.; Roux, S.; Tillement, O. *J. Am. Chem. Soc.* **2008**, *130*, 5908; (c) Moriggi, L.; Cannizzo, C.; Dumas, E.; Mayer, C. R.; Ylianov, A.; Helm, L. *J. Am. Chem. Soc.* **2009**, *131*, 10828.
9. (a) Dutta, S.; Kim, S.-K.; Patel, D. B.; Kim, T.-J.; Chang, Y.-M. *Polyhedron* **2007**, *26*, 3799; (b) Dutta, S.; Park, J.-A.; Jung, J.-C.; Chang, Y.-M.; Kim, T.-J. *Dalton Trans.* **2008**, *16*, 2199; (c) Park, J.-A.; Lee, J.-J.; Jung, J.-C.; Yu, D.-Y.; Oh, C.; Ha, S.; Kim, T.-J.; Chang, Y. *ChemBioChem* **2008**, *9*, 2811; (d) Park, J.-A.; Reddy, P. A. N.; Kim, H.-K.; Kim, I.-S.; Kim, G.-C.; Chang, Y.; Kim, T.-J. *Bioorg. Med. Chem. Lett.* **2008**, *18*, 6135.
10. Grabar, K. C.; Freeman, R. G.; Hommer, M. B.; Natan, M. J. *Anal. Chem.* **1995**, *67*, 735.
11. Joint Committee on Powder Diffraction Standards (JCPDS) Card No. 04-0784, 2002.
12. (a) Chechik, V.; Crooks, R. M. *Langmuir* **1999**, *15*, 6364; (b) Johnson, S. R.; Evans, S. D.; Mahon, S. W.; Ulman, A. *Langmuir* **1997**, *13*, 51.
13. (a) Daniel, M.-C.; Astruc, D. *Chem. Rev.* **2004**, *104*, 293; (b) Yonezawa, T.; Kunitake, T. *Coll. Surf. A.* **1999**, *149*, 193.
14. Lewis, D.; Day, T. M.; MacPherson, J. V.; Pikramenou, Z. *Chem. Commun.* **2006**, 1433.
15. (a) Gierada, D. S.; Bae, K. T. *Radiology* **1999**, *210*, 829; (b) Bloem, J. L.; Wondergem, J. *Radiology* **1989**, *171*, 578.
16. (a) De Jong, W. H.; Hagens, W. I.; Krystek, P.; Burger, M. C.; Sips, A. J. A. M.; Geertsma, R. E. *Biomaterials* **2008**, *29*, 1912; (b) Hillyer, J. F.; Albrecht, R. M. *Microsc. Microanal.* **1999**, *4*, 481.
17. (a) Terentyuk, G. S.; Maslyakova, G. N.; Suleymanova, L. V.; Khlebtsov, B. N.; Kogan, B. Y.; Akchurin, G. G.; Shantrocha, A. V.; Maksimova, I. L.; Khlebtsov, N. G.; Tuchin, V. V. *J. Biophoton* **2009**, *2*, 292; (b) Sonavane, G.; Tomoda, K.; Makino, K. *Coll. Surf. B.* **2008**, *66*, 274.
18. Kim, J. S.; Rieter, W. J.; Taylor, K. M. L.; An, H.; Lin, W. *J. Am. Chem. Soc.* **2007**, *129*, 8962.
19. (a) Yan, G.-P.; Robinson, L.; Hogg, P. *Radiography* **2007**, *13*, e5; (b) Shamsi, K.; Balzer, T.; Saini, S. *Radiology* **1998**, *206*, 365.
20. Lin, J.-J.; Chen, J.-S.; Huang, S.-J.; Ko, J.-H.; Wang, Y.-M.; Chen, T.-L.; Wang, L.-F. *Biomaterials* **2009**, *30*, 5114.
21. Connor, E. E.; Mwamuka, J.; Gole, A.; Murphy, C. J.; Wyatt, M. D. *Small* **2005**, *1*, 325.